"Regrowth-Free" Fabrication of High-current-gain AlGaN/GaN Heterojunction Bipolar Transistor with N-p-n Configuration

Takeru Kumabe[1*], Hirotaka Watanabe[2], Yuto Ando[2], Atsushi Tanaka[2], Shugo Nitta[2], Yoshio Honda[2], and Hiroshi Amano[2,3,4]

[1]*Department of Electronics, Nagoya University, Nagoya 464-8603, Japan*

[2]*Institute of Materials and Systems for Sustainability, Nagoya University, Nagoya 464-8601, Japan*

[3]*Venture Business Laboratory, Nagoya University, Nagoya 464-8603, Japan*

[4]*Akasaki Research Center, Nagoya University, Nagoya 464-8601, Japan*

E-mail: kumabe@nagoya-u.jp

An AlGaN/GaN heterojunction bipolar transistor (HBTs) with N-p-n configuration was fabricated by the "regrowth-free" method, resulting in a contamination-free emitter-base AlGaN/GaN heterojunction. The low-bias-power-based low-damage inductively coupled plasma–reactive ion etching was employed in this study for emitter mesa definition instead of the conventional selective-area-regrowth technique. The method successfully minimized the etching-induced damage in the p-GaN base layer and the contamination at the emitter-base AlGaN/GaN heterojunction. Consequently, the fabricated device exhibited a high current gain of 25, the highest current density of 15.0 kA/cm^2, and the lowest on-state voltage offset of 0.75 V ever reported for AlGaN/GaN HBTs.

Keywords; GaN, AlGaN, heterojunction bipolar transistors, regrowth-free, Dry etching

Gallium nitride (GaN)-based heterojunction bipolar transistors (HBTs) are a promising device for next-generation communication technologies thanks to their high power-handling capability, good linearity, and normally-off characteristics[1–3]. To date, indium gallium nitride (InGaN)/GaN HBTs have demonstrated the excellent DC characteristics of high current gain (> 100), high current density (~15 kA/cm^2), and small collector-emitter offset voltage (< 1 V) [4–8]. In addition, RF operations with the cutoff frequency (f_T) and the maximum oscillation frequency (f_{Max}) of 5.3 GHz and 1.3 GHz, respectively, have also been demonstrated thanks to the high hole concentration and low sheet resistance of p-InGaN used as a base layer [8,9]. Although InGaN/GaN HBTs have exhibited such good performance, “V-shaped” defects at the heterointerface owing to the large lattice mismatch of InGaN to GaN are the bottleneck from the viewpoint of reducing leakage current and improving current gain[10]. On the other hand, aluminum gallium nitride (AlGaN)/GaN HBTs attract attention for their low leakage current and large current gain compared with those of InGaN/GaN HBTs thanks to the smaller lattice mismatch of AlGaN to GaN[11–15]. For AlGaN/GaN HBTs with the N-p-n configuration, the emitter region is generally fabricated by selective-area regrowth because of the difficulty of reducing etching-induced damage in the base (p-GaN) and making an excellent metal/p-GaN contact onto the etched surface[16,17]. However, it is a critical issue in the conventional method that the deterioration of device characteristics including reverse leakage current is caused by unintentional impurity doping (Si, O, and sometimes Fe) at the emitter-base heterointerface during the initial step of the regrowth process[18,19]. To further develop AlGaN/GaN HBTs, “regrowth-free” fabrication processes that enable the formation of high-quality emitter-base heterointerfaces by low-damage etching should be established.

Recently, we have reported inductively coupled plasma–reactive ion etching (ICP–RIE)-induced damage in heavily Mg-doped p-GaN and the critical ICP–RIE parameter to suppress this damage[20]. This study applied the low-damage ICP–RIE to fabricate AlGaN/GaN HBTs with N-p-n configuration grown simultaneously (i.e., fabricated without any regrowth process). The fabricated devices exhibited a common-emitter current gain (β) of 25 and a maximum current density (J_{CMax}) of 15.0 kA/cm^2, which are equal to or better than those of devices fabricated via the regrowth process.

Figure 1 illustrates the schematic cross-sectional view of a fabricated AlGaN/GaN HBT with the N-p-n configuration. The layer structure was simultaneously grown by metal-organic vapor phase epitaxy on a *c*-plane free-standing Si-doped n-GaN substrate ([Si] =

1.1×10^{18} cm^{-3}) with a threading dislocation density (TDD) of 1.7×10^{6} cm^{-2}. From the substrate up, it consists of a 1.1-μm-thick Si-doped n-GaN sub-collector ([Si] = 1.7×10^{18} cm^{-3}), a 1.7-μm-thick n^{-}-GaN collector ([Si] = 6.9×10^{16} cm^{-3}), a-100-nm thick Mg-doped p^{+}-GaN base ([Mg] = 8.9×10^{18} cm^{-3}), a 75-nm-thick n^{+}-AlGaN emitter (AlN mole fraction of 14.8%, [Si] = 1.8×10^{19} cm^{-3}), and a 65-nm-thick n-GaN cap ([Si] = 6.5×10^{18} cm^{-3}). The Si and Mg concentration depth profiles were determined by secondary ion mass spectroscopy (SIMS), and the AlN mole fraction of the AlGaN layer was evaluated by X-ray diffraction reciprocal (XRD). The detailed result and discussions for the SIMS and XRD-RSM are summarized in supplementary contents. Negatively beveled base mesa and vertical emitter mesa structures were formed by Cl_2-based ICP–RIE. During the final 80 nm of emitter mesa etching (p-GaN exposure etching), the ICP–RIE bias power was precisely controlled at a low level (~2.5 W) to minimize etching-induced damage of p^{+}-GaN[20–22]. Subsequently, annealing was performed at 1123 K in N_2 ambient to dehydrogenate and activate Mg atoms as acceptors. In the activation annealing process, the treatment time was set to be as long as 90 min to promote the lateral diffusion of H atoms in the p^{+}-GaN layer sandwiched by n-type layers[23,24]. For ohmic contacts to the base and the emitter, Ni/Au and Ti/Al/Ti/Au metal stacks were deposited and sintered, respectively. A 200-nm-thick SiO_2 layer passivated the surface, and the contact holes were opened by wet etching using buffered hydrofluoric acid. Finally, Ti/Au and Al/Au were deposited on the device surface and the backside of the substrate as the pad and the collector ohmic electrode, respectively. DC characteristics of the fabricated HBTs were examined using a Keysight B1500A semiconductor parameter analyzer at room temperature.

The sheet resistance (R_{SH}) of the etched base layer (p^{+}-GaN) was first evaluated by the transfer length method (TLM) [25]. Figure 2(a) shows the schematic illustration of a fabricated TLM test structure. The layer thickness determined by comparing the etched depth and SIMS result was about 70 nm. Current–voltage (I–V) characteristics of two terminals with different contact distances (W_{gap}) in the range of 3–20 μm and total resistance (R_T, sum of contact resistance and bulk resistance between electrodes) as a function of W_{gap} are summarized in Figs. 2(b) and 2(c), respectively. Since the metal–semiconductor contact exhibited non-Ohmic behavior, the values of R_T were calculated by differentiating a voltage by a current at 5 V where it was in the series-resistance dominant region (i.e., the sheet resistance is the major current limiting factor in this structure) [26]. Despite the non-Ohmic behavior, clear W_{gap} dependence of R_T, which could not be seen in the damaged sample, was observed. The

R_{SH} extracted from the R_T–W_{gap} plot by least-squares fitting was 458 kΩ/sq., which was within the same order as the theoretical value of 320 kΩ/sq. assuming a hole concentration (p) of 1.39×10^{17} cm^{-3} and a hole mobility (μ_p) of 20 $cm^2V^{-1}s^{-1}$ [27–29]. Those results indicate that a nearly damage-free p^+-GaN base layer, essential for bipolar operation, can be obtained by utilizing low-bias-power ICP–RIE in the mesa formation process.

Figure 3 shows the Gummel plot of a fabricated AlGaN/GaN HBT. The device had a 10 µm × 10 µm emitter area, and the base-collector voltage (V_{BC}) was fixed at 0 V during the measurement. The current gain (β) was calculated by dividing the collector current (I_C) by the base current (I_B) at each base-emitter voltage (V_{BE}). The device exhibited current amplification above V_{BE} = 5.36 V. It achieved the maximum current gain (β_{Max}) of 25, almost ten times as high as any reported Npn-type AlGaN/GaN HBT fabricated without any regrowth processes[30,31]. In addition, the maximum current density (J_{CMax}) was as high as 15.0 kA/cm^2, which is the record value in AlGaN/GaN HBTs compared with the highest value of 8 kA/cm^2 [17] and is comparable to those of InGaN/GaN HBTs (~15 kA/cm^2) [7,8]. From the SIMS and XRD-RSM analyses, unintentionally doped Si, Fe, and C concentrations were negligible around the AlGaN/GaN heterointerface, and the AlGaN emitter layer was perfectly strained on the GaN substrate. The nearly ideal emitter-base hetero-junction resulted in excellent current gain and current density.

Figure 4 shows the common-emitter I–V characteristics of a fabricated AlGaN/GaN HBT. The base current was varied in the range of 0–100 µA in 10 µA steps. The device showed good saturation properties with a leakage current at I_B = 0 A of almost the detection limit in the measurement system. The collector-emitter offset voltage (V_{offset}) extracted from the output characteristics was as low as 0.75 V. Although V_{offset} was higher than the theoretical value of < 0.2 V in this structure, it was less than or close to that of those reported for AlGaN/GaN HBTs (~2 V) [16,32,33] and InGaN/GaN HBTs (~0.3 V) [7,8]. McCarthy *et al.* proposed the mechanism behind the large V_{offset} observed in the III-N-based HBTs to be the voltage drop associated with the metal/p-GaN contact and the bulk sheet resistance[1]. As we described in the previous report[20], our metal/p-GaN contact on the etched surface was similar to the unetched one because of the reduced thickness in the damaged layer. Therefore, the small voltage drop in the damaged layer at the interface contributed to our relatively low V_{offset}. Furthermore, the doping concentration and width of the p^+-GaN base layer underneath the n^+-AlGaN emitter layer were evaluated utilizing the Early voltage (V_A) extracted from the I_C–V_{CE} characteristics. Figure 5 shows the extraction of the V_A from the I_C–V_{CE} characteristics (shown in Fig. 4). The extracted V_A value was about 156 V, and it was determined from I_C curves corresponding to the I_B range of 10–50 μA since slight distortions were observed in I_C curves corresponding to I_B higher than 60 μA. In uniformly doped base bipolar transistors, V_A is given by

$$V_{\mathrm{A}} = \frac{q N_{\mathrm{B}} W_{\mathrm{B}}^2}{\epsilon_{\mathrm{s}} \epsilon_0} \tag{1}$$

where q is the elementary charge, N_B is the net acceptor concentration in the base layer, W_B is the base width (thickness of the base layer), ε_s is the relative permittivity of the semiconductor, and ε_0 is the vacuum permittivity[34)]. Considering the SIMS result of N_B = [Mg] = 8.9×10^{18} cm^{-3}, W_B = 100 nm, and $\varepsilon_s = 10.4\varepsilon_0$ [35)], the projected V_A of the fabricated device structure was 156 V, which was in good agreement with the experimental value of 160 V. The result also supports the outcome of TLM analysis and indicates that a nearly ideal p-GaN bulk with complete dehydrogenation (N_A = [Mg]) can be obtained as a base layer even by the "regrowth-free" fabrication process.

In conclusion, we have fabricated AlGaN/GaN HBTs with the N-p-n configuration by the "regrowth-free" process based on low-damage ICP–RIE. The TLM and device characteristic V_A implied that a nearly damage-free p-GaN bulk in the base layer was realized. The fabricated AlGaN/GaN HBTs exhibited the high β_{Max} of 25, the highest J_{CMax} of 15.0 kA/cm^2, and the lowest V_{offset} of 0.7 V ever reported for AlGaN/GaN HBTs with good saturation properties. The results suggest that the "regrowth-free" fabrication could resolve the bottlenecks of AlGaN/GaN HBTs, including the huge contact resistance of metal/p-GaN and contaminations at the AlGaN/GaN heterointerface. By further reducing the metal/p-GaN contact resistance and optimizing the device layout, regrowth-free fabrication can open a path to RF AlGaN/GaN HBTs for the next-generation communication technology.

Acknowledgments

This research was supported by the Japan Ministry of the Environment through the project of GaN technology innovation for enabling decarbonized society and lifestyle, and JSPS KAKENHI under Grant No. 21J22909. The authors would like to acknowledge Mr. Seiya Kawasaki and Prof. Manato Deki of Nagoya University for their invaluable discussion and considerable support.

References

1) L. S. McCarthy, I. P. Smorchkova, H. Xing, P. Kozodoy, P. Fini, J. Limb, D. L. Pulfrey, J. S. Speck, M. J. W. Rodwell, S. P. DenBaars, and U. K. Mishra, IEEE Trans. Electron Devices **48(3)**, 543 (2001).
2) S.-C. Shen, R. D. Dupuis, Z. Lochner, Y.-C. Lee, T.-T. Kao, Y. Zhang, H.-J. Kim, and J.-H. Ryou, Semicond. Sci. Technol. **28**, 074025 (2013).
3) R. D. Dupuis, J. Kim, Y.-C. Lee, Z. Lochner, M.-H. Ji, T.-T. Kao, J.-H. Ryou, T. Detchphrom, and S.-C. Shen, ECS Trans. **58**, 261 (2013).
4) T. Makimoto, K. Kumakura, and N. Kobayashi, Appl. Phys. Lett. **83**, 1035 (2003).
5) T. Makimoto, Y. Yamauchi, and K. Kumakura, Appl. Phys. Lett. **84**, 1964 (2004).
6) Y.-C. Lee, Y. Zhang, Z. M. Lochner, H.-J. Kim, J.-H. Ryou, R. D. Dupuis, and S.-C. Shen, Phys. Status Solidi A **209(3)**, 497 (2012).
7) Z. Lochner, H. J. Kim, Y.-C. Lee, Y. Zhang, S. Choi, S.-C. Shen, P. D. Yoder, J.-H. Ryou, and R. D. Dupuis, Appl. Phys. Lett. **99**, 193501 (2011).
8) S.-C. Shen, R. D. Dupuis, Y.-C. Lee, H.-J. Kim, Y. Zhang, Z. Lochner, P. D. Yoder, and J.-H. Ryou, IEEE Electron Device Lett. **32(8)**, 1065 (2011).
9) K. Kumakura, T. Makimoto, and N. Kobayashi, J. Cryst. Growth **221**, 267 (2000).
10) T. Chung, J. Limb, J.-H. Ryou, W. Lee, P. Li, D. Yoo, X.-B. Zhang, P. Asbeck, B. Chukung, M. Feng, D. Zakharov, and Z. Lilienthal-Weber, J. Electron. Mater. **35(4)**, 695 (2006).
11) G. Martin, S. Strite, A. Botchkarev, A. Agarwal, A. Rockett, H. Morkoç, W. R. L. Lambrecht, and B. Segall, Appl. Phys. Lett. **65**, 610 (1994).
12) G. Martin, A. Botchkarev, A. Rockett, and H. Morkoç, Appl. Phys. Lett. **68**, 2541 (1996).
13) H. Angerer, B. Brunner, F. Freudenberg, O. Ambacher, M. Stutzmann, R. Höpler, T. Metzger, E. Born, G. Dollinger, A. Bergmaier, S. Karsch, and H.-J. Körner, Appl. Phys. Lett. **71**, 1504 (1997).
14) O. Ambacher, B. Foutz, J. Smart, J. R. Shealy, N. G. Weimann, K. Chu, M. Murphy, A. J. Sierakowski, W. J. Schaff, L. F. Eastman, R. Dimitrov, A. Mitchell, and M. Stutzmann, J. Appl. Phys. **87**, 334 (2000).
15) I. Vurgaftman and J. R. Meyer, J. Appl. Phys. **94**, 3675 (2003).
16) H. Xing, P. M. Chavarkar, S. Keller, S. P. DenBaars, and U. K. Mishra, IEEE Electron Device Lett. **24(3)**, 141 (2003).
17) L. Zhang, Z. Cheng, J. Zeng, H. Lu, L. Jia, Y. Ai, and Y. Zhang, IEEE Trans. Electron

Devices **66(3)**, 1197 (2019).

18) H. Xing, S. P. DenBaars, and U. K. Mishra, J. Appl. Phys. **97**, 113703 (2005).

19) K. Fu, H. Fu, H. Liu, S. R. Alugubelli, T.-H. Yang, X. Huang, H. Chen, I. Baranowski, J. Montes, F. A. Ponce, and Y. Zhao, Appl. Phys. Lett **113**, 233502 (2018).

20) S. Yamada, M. Omori, H. Sakurai, Y. Osada, R. Kamimura, T. Hashizume, J. Suda, and T. Kachi, Appl. Phys. Express **13**, 016505 (2020).

21) S. Yamada, K. Takeda, M. Toguchi, H. Sakurai, T. Nakamura, J. Suda, T. Kachi, and T. Sato, Appl. Phys. Express **13**, 106505 (2020).

22) T. Kumabe, Y. Ando, H. Watanabe, M. Deki, A. Tanaka, S. Nitta, Y. Honda, and H. Amano, Jpn. J. Appl. Phys. **60**, SBBD03 (2021).

23) Y. Kuwano, M. Kaga, T. Morita, K. Yamashita, K. Yagi, M. Iwaya, T. Takeuchi, S. Kamiyama, and I. Akasaki, Jpn. J. Appl. Phys. **52**, 08JK12 (2013).

24) T. Narita, K. Tomita, S. Yamada, and T. Kachi, Appl. Phys. Express **12**, 011006 (2019).

25) D. K. Schroder, *Semiconductor Material and Device Characterization* (Wiley, New Jersey, 2006) 3rd ed., p. 138.

26) R. Piotrzkowski, E. Litwin-Staszewska, and Sz. Grzanka, Appl. Phys. Lett. **99**, 052101 (2011).

27) P. Kozodoy, H. Xing, S. P. DenBaars, U. K. Mishra, A. Saxler, R. Perrin, S. Elhamri, and W. C. Mitchel, J. Appl. Phys. **87**, 1832 (2000).

28) M. Horita, S. Takashima, R. Tanaka, H. Matsuyama, K. Ueno, M. Edo, T. Takahashi, M. Shimizu, and J. Suda, Jpn. J. Appl. Phys. **56**, 031001 (2017).

29) T. Narita, N. Ikarashi, K. Tomita, K. Kataoka, and T. Kachi, J. Appl. Phys. **124**, 165706 (2018).

30) F. Ren, J. Han, R. Hickman, J. M. Van Hove, P. P. Chow, J. J. Klaassen, J. R. LaRoche, K. B. Jung, H. Cho, X. A. Cao, S. M. Donovan, R. F. Kopf, R. G. Wilson, A. G. Baca, R. J. Shul, L. Zhang, C. G. Willison, C. R. Abernathy, and S. J. Pearton, Solid-State Electronics **44**, 239 (2000).

31) Y. T. Tseng, C. W. Lin, W. C. Yang, K. Y. Chen, and K. Y. Cheng, IEEE Trans. Electron Devices **63(11)**, 4262 (2016).

32) J. B. Limb, L. McCarthy, P. Kozodoy, H. Xing, J. Ibbetson, Y. Smorchkova, S. P. DenBaars, and U. K. Mishra, Electron. Lett. **35(19)**, 1671 (1999).

33) L. S. McCarthy, P. Kozodoy, M. J. W. Rodwell, S. P. DenBaars, and U. K. Mishra, IEEE Electron Device Lett. **20(6)**, 277 (1999).

34) Y. Taur and T. H. Ning, *Fundamentals of Modern VLSI Devices* (Cambridge Univ. Press,

Cambridge, 2009) 2nd ed., p.340.

35) A. S. Barker, Jr. and M. Ilegems, Phys. Rev. B **7(2)**, 743 (1972).

Figure Captions

Fig. 1. Schematic cross-sectional view of fabricated AlGaN/GaN HBT with N-p-n configuration.

Fig. 2. (a) Schematic illustration of fabricated TLM test structure. (b) Current–voltage (*I*–*V*) characteristics of two terminals with contact distance (W_{gap}) of 3–20 µm. (c) Total resistance (R_T) as a function of W_{gap}.

Fig. 3. Gummel plot of fabricated AlGaN/GaN HBT. The base-collector voltage (V_{BC}) was fixed at 0 V during the measurement.

Fig. 4. Common-emitter *I*–*V* characteristics of a fabricated AlGaN/GaN HBT. The base current (I_B) was varied in the range of 0–100 µA in 10 µA steps.

Fig. 5. Extraction of Early voltage from common-emitter *I*–*V* characteristics of a fabricated AlGaN/GaN HBT.

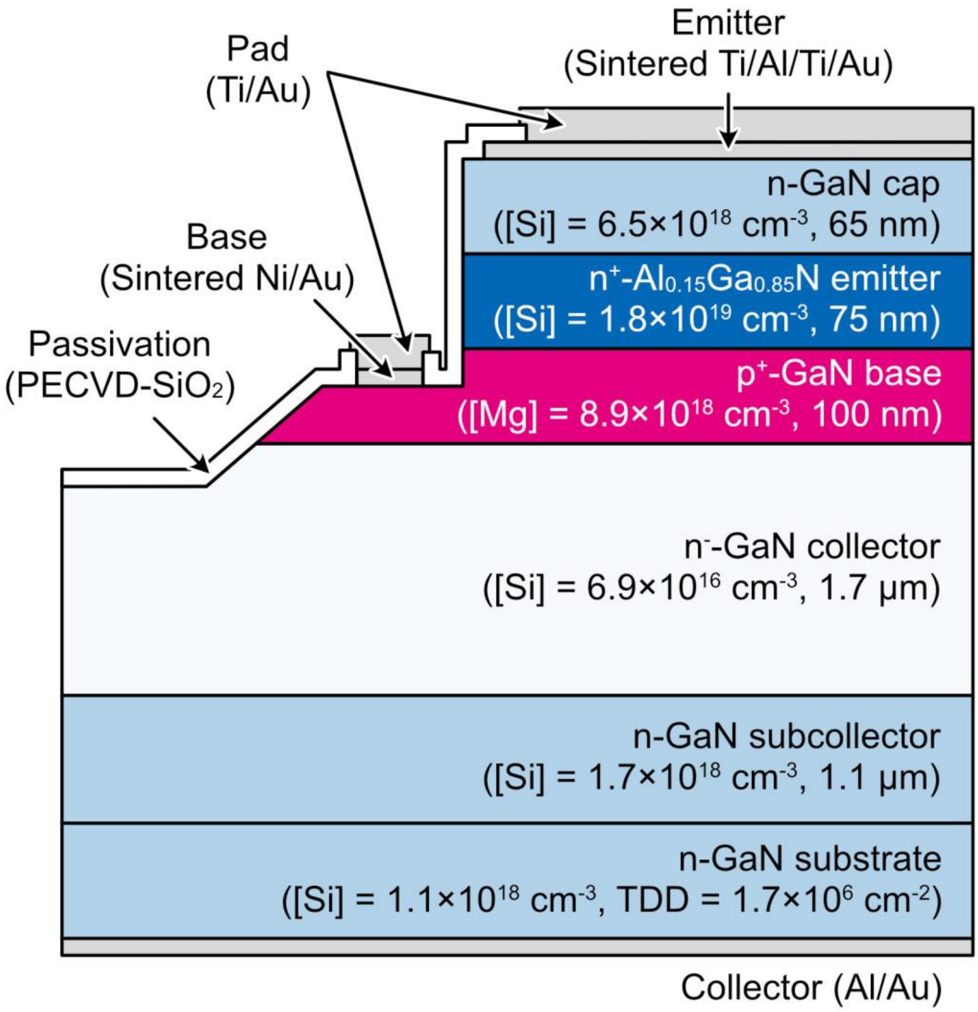
Emitter
(Sintered Ti/Al/Ti/Au)
Pad
(Ti/Au)
n-GaN cap
([Si] = 6.5×10^18 cm^-3, 65 nm)
Base
(Sintered Ni/Au)
n+-Al0.15Ga0.85N emitter
([Si] = 1.8×10^19 cm^-3, 75 nm)
Passivation
(PECVD-SiO2)
p+-GaN base
([Mg] = 8.9×10^18 cm^-3, 100 nm)
n--GaN collector
([Si] = 6.9×10^16 cm^-3, 1.7 μm)
n-GaN subcollector
([Si] = 1.7×10^18 cm^-3, 1.1 μm)
n-GaN substrate
([Si] = 1.1×10^18 cm^-3, TDD = 1.7×10^6 cm^-2)
Collector (Al/Au)

Fig. 1

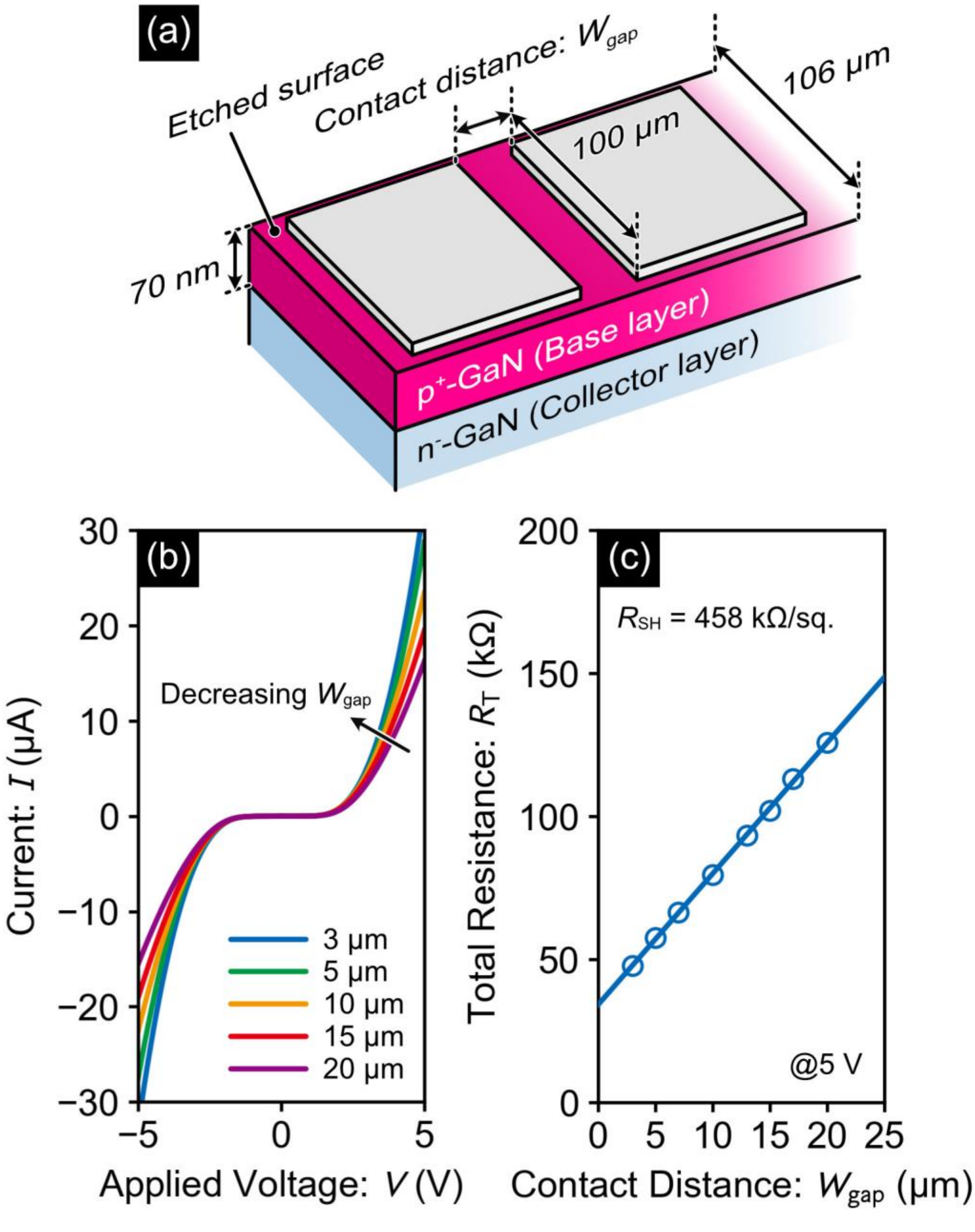
(a)
Etched surface
Contact distance: W_{gap}
106 µm
100 µm
70 nm
p^+-GaN (Base layer)
n^--GaN (Collector layer)
(b)
Decreasing W_{gap}
3 µm
5 µm
10 µm
15 µm
20 µm
Current: I (µA)
Applied Voltage: V (V)
(c)
R_{SH} = 458 kΩ/sq.
@5 V
Total Resistance: R_T (kΩ)
Contact Distance: W_{gap} (µm)

Fig. 2

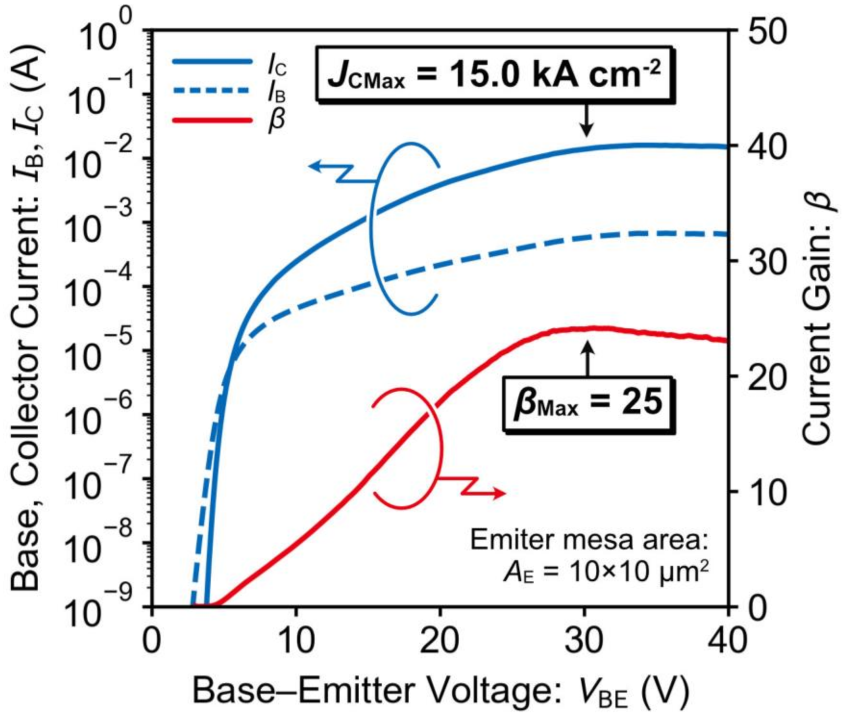

I_C
I_B
β
J_{CMax} = 15.0 kA cm^{-2}
β_{Max} = 25
Emiter mesa area:
A_E = 10×10 μm^2
Base, Collector Current: I_B, I_C (A)
Current Gain: β
Base–Emitter Voltage: V_{BE} (V)
10^0
10^{-1}
10^{-2}
10^{-3}
10^{-4}
10^{-5}
10^{-6}
10^{-7}
10^{-8}
10^{-9}
0
10
20
30
40
50

Fig. 3

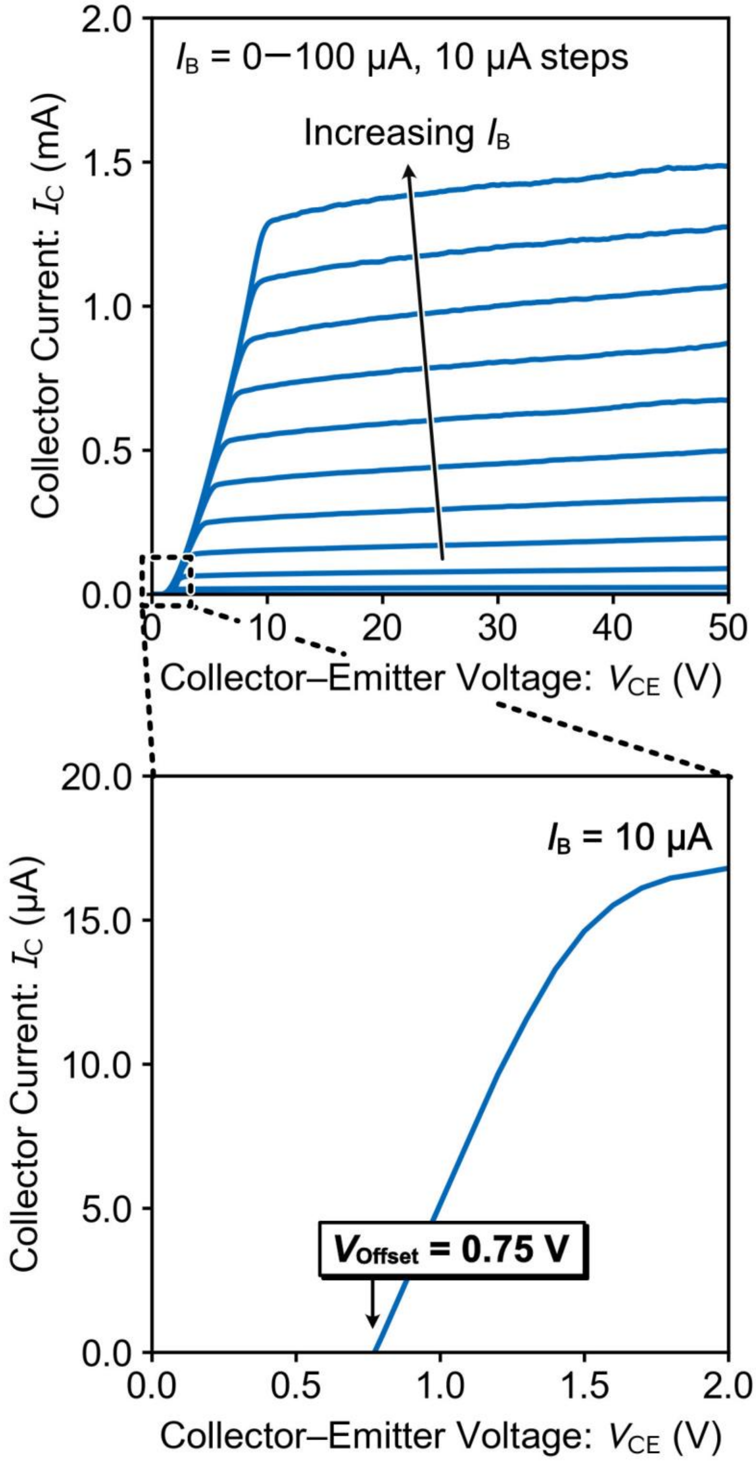

2.0
1.5
1.0
0.5
0.0
Collector Current: I_C (mA)
I_B = 0−100 μA, 10 μA steps
Increasing I_B
0
10
20
30
40
50
Collector–Emitter Voltage: V_{CE} (V)
20.0
15.0
10.0
5.0
0.0
Collector Current: I_C (μA)
I_B = 10 μA
V_{Offset} = 0.75 V
0.0
0.5
1.0
1.5
2.0
Collector–Emitter Voltage: V_{CE} (V)

Fig. 4

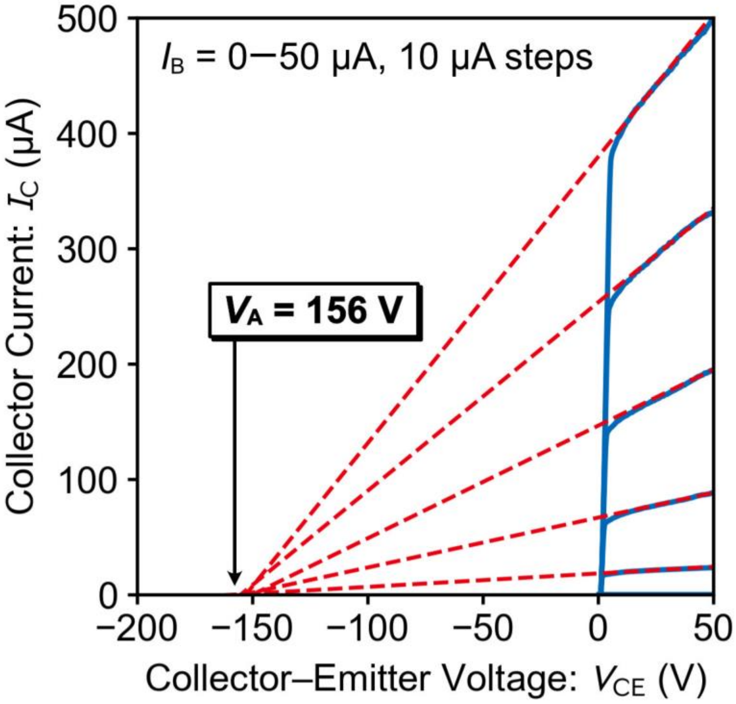

I_B = 0−50 μA, 10 μA steps
V_A = 156 V
Collector Current: I_C (μA)
Collector–Emitter Voltage: V_{CE} (V)
0
100
200
300
400
500
−200
−150
−100
−50
0
50

Fig. 5